Check for updates

Research Article | Vol. 30, No. 3 / 31 Jan 2022 / Optics Express 3954

Optics EXPRESS

Up to 300 K lasing with GeSn-On-Insulator microdisk resonators

A. Bjelajac,[1] M. Gromovyi,[1] E. Sakat,[1] B. Wang,[1] G. Patriarche,[1] N. Pauc,[2] V. Calvo,[2] P. Boucaud,[3] F. Boeuf,[4] A. Chelnokov,[5] V. Reboud,[5] M. Frauenrath,[5] J.-M. Hartmann,[5] and M. El Kurdi[1,*]

[1] *Université Paris-Saclay, CNRS, C2N, 10 boulevard Thomas Gobert, 91120 Palaiseau, France*
[2] *Université Grenoble Alpes, CEA, IRIG-DePhy, 17 rue des Martyrs, 38000 Grenoble, France*
[3] *Université Côte d'Azur, CNRS, CRHEA, Rue Bernard Grégory, 06905 Sophia-Antipolis, France*
[4] *STMicroelectronics, Rue Jean Monnet, 38054 Crolles, France*
[5] *Université Grenoble Alpes, CEA, Leti, 17 rue des Martyrs, 38000 Grenoble, France*
[*] *moustafa.el-kurdi@c2n.upsaclay.fr*

Abstract: GeSn alloys are the most promising direct band gap semiconductors to demonstrate full CMOS-compatible laser integration with a manufacturing from Group-IV materials. Here, we show that room temperature lasing, up to 300 K, can be obtained with GeSn. This is achieved in microdisk resonators fabricated on a GeSn-On-Insulator platform by combining strain engineering with a thick layer of high Sn content GeSn.

© 2022 Optica Publishing Group under the terms of the Optica Open Access Publishing Agreement

1. Introduction

The first demonstration of low-temperature lasing with direct band gap GeSn, published in 2015 [1], was followed by several breakthroughs like electrically-injected lasing up to 100 K [2] and continuous wave (CW) laser operation up to 70 K [3]. An important milestone towards real-field applications is the ability to operate at room temperature (RT). A critical parameter to have a performant laser at high temperature is the directness of the band structure, defined as the energy barrier between the zone center (Γ) and the indirect (L) valleys of the conduction band. This energy barrier should typically be around 150-200 meV, to maintain the Γ-state electron population up to room temperature and have an optical gain involving direct transitions with the valence band hole states [4]. To reach such directness, a high amount of tin (Sn) in the alloys is required, of the order of 16%. Such high Sn contents are challenging to achieve. In practice, the use of Ge strain relaxed buffers (SRBs) on silicon was proven to be most appropriate to grow GeSn alloys and mitigate the large lattice mismatch with Si substrates. However, increasing the Sn content results in a large compressive strain that reduces the band gap directness and degrades the gain. The mainstream approach, to overcome compressive strain issues, is to grow layers definitely above their critical thickness for plastic relaxation, with a strain relaxation typically around 75%. [5] However, dense arrays of misfit dislocations near the GeSn/Ge SRB interface are then formed, resulting in non-radiative processes detrimental to lasing [6]. So far, the highest temperatures achieved for laser operation were 273 K for 16% of Sn and 270 K for 17% of Sn, although the directness parameter was expected then to be high enough to reach RT lasing in [7] and [8]. In Ref. [7], bandgap directness was reinforced by some uniaxial strain.

To go to higher temperatures, we propose a strategy relying on a specific GeSn-On-Insulator (GeSnOI) mesa structure with the use of SiN as stressor as recently proposed in Ref. [9]. The GeSnOI stack is fabricated with layer bonding onto a metallic film for improved thermal management [10]. The main assets of this platform is, first, to enable the removal of the GeSn/Ge SRB interfacial defects by simple etching after bonding. Second, the optical confinement is improved compared to conventional GeSn /Ge SRB stacks thanks to the higher optical index

#449895 https://doi.org/10.1364/OE.449895
Journal © 2022 Received 1 Dec 2021; revised 11 Jan 2022; accepted 11 Jan 2022; published 21 Jan 2022

Optics EXPRESS

contrast between GeSn and the SiN layer underneath. Third, the strain transfer yields a higher directness of the alloy [4]. The combination of these advantages leads to RT lasing in microdisk resonators, as shown in the following.

2. Fabrication

Our strategy was to use a 720 nm thick GeSn layer with 16.9% of Sn on top of a 2.5 µm thick Ge SRB, itself on a silicon (Si) (001) substrate. A $Ge_2H_6 + SnCl_4$ chemistry was used to grow that layer, at 313°C, 100 Torr with a growth rate of 22 nm/min. Reciprocal Space Maps around the (004) and (224) X-Ray Diffraction orders gave us access to the Sn concentration and macroscopic degree of strain relaxation R of that GeSn layer. As expected from [11], we had some Sn enrichment in the GeSn layer as soon as the built-in compressive strain started to plastically relax. This resulted in a higher Sn content, less compressively strained GeSn layer (16.9%, $R = 84\%$) on top of a lower Sn content, more dislocated and almost fully relaxed GeSn layer (13.3%, $R = 98\%$), as shown in Fig. 1. The residual compressive strain in the top, optically active part of the GeSn layer was thus -0.5%. Meanwhile, the Ge SRB underneath was slightly tensile strained. This was due to thermal dilatations coefficients' differences between the fully relaxed Ge SRB and the Si substrate that came into play during the cooling-down to room temperature after growth [12]. This was the reason why the Ge SRB peak was not, in Fig. 1(a), on the Si fully Relaxed Line.

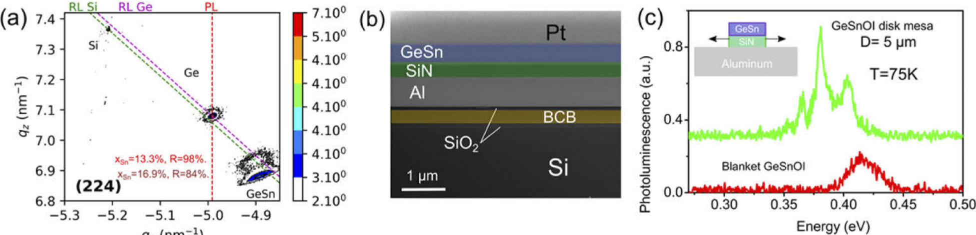

Fig. 1. (a) Reciprocal Space Map around the (224) X-Ray Diffraction order gave access to the in-plane and out-of-plane lattice parameter of the bottom and top parts of the thick GeSn layer on the Ge-buffered Si(001) substrate and thus, to their Sn contents and macroscopic degrees of strain relaxation ([Sn] 13.3% and $R = 98\%$ and [Sn] 16.9% and $R = 84\%$). RL are acronyms for the fully Relaxed Lines (from the origin of the reciprocal space to the Si or the Ge peaks ; if the GeSn layers were fully relaxed, they would be on the Ge RL). Meanwhile, PL is an acronym for the Pseudomorphic Line (same in-plane lattice parameter and thus, same q_x coordinate than the Ge SRB; if the GeSn layers were fully strained on the Ge SRB underneath, they would be on that vertical line). (b) cross-sectional scanning electron microscope image of the GeSnOI stack (after bonding with BenzoCycloButene (BCB) on a Si wafer) showing the active GeSn layer, the SiN stressor and the Al heat sink. The Pt layer on top was used to protect the surface during the Focused Ion Beam (FIB) etching of microdisk mesas. (c) 75 K photoluminescence spectra under continuous-wave optical pumping of blanket GeSnOI and of a GeSnOI microdisk mesa. The spectrum of the latter was vertically offset for clarity purposes. The microdisk emission is strongly modulated by cavity resonances.

The GeSnOI layer was thinned down after bonding, with therefore a removal of interfacial defects (Fig. 1(b)). The overall thermal budget was lowered as much as possible, as thermal stress could result in local Sn precipitation [13]. Bonding, which lasted 30 minutes, was thus performed at a temperature of 210°C, i.e. far below the GeSn growth temperature of 313°C (and a similar duration). The final bonded layer thickness was 450 nm and we did follow the procedure recommended by the supplier for the bonding. In the following, we will assume that the Sn composition was the same in microdisks than in the epitaxial stack, as we did not observe

any precipitation by transmission electron microscopy. After patterning into microdisk mesa, the layer became slightly tensile-strained by the bottom SiN stressor layer, by 0.1%, typically. The in-plane strain change, from -0.5% to 0.1%, resulted in a red shift, by typically 40 meV, of the photoluminescence emission spectrum for the microdisk mesa as compared to the one of the blanket GeSnOI stack (Fig. 1(c)) [9]. The emission spectrum of the microdisk mesa showed typical cavity resonance patterns that were not present on the blanket photoluminescence spectrum. The 40 meV shift was estimated from the envelope of the photoluminescence spectra, i.e. without accounting for the resonances.

3. Optically pumped laser characterizations

Figure 2 shows a scanning electron microscopy (SEM) image of a microdisk mesa resonator fabricated from the GeSnOI stack. The emission from the cavities is optically excited and analyzed as a function of temperature and excitation power density using the setup and excitation conditions shown in Fig. 2. Emission spectra at 293 K (20°C) from a 5 μm diameter GeSnOI microdisk mesa under 400 kW cm^{-2} and 800 kW cm^{-2} pulsed excitation densities in Fig. 2 show a clear change from a broad spontaneous emission regime to lasing.

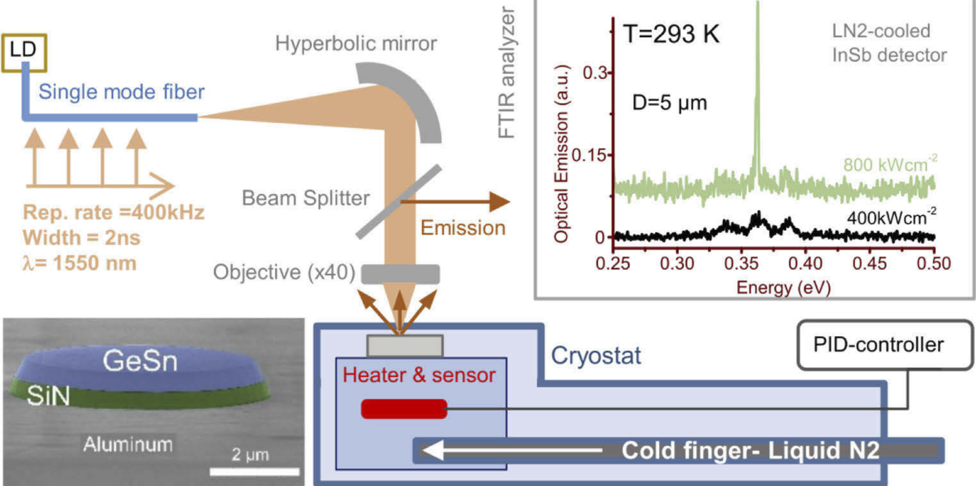

Fig. 2. Experimental set-up. A SEM image of a GeSnOI microdisk mesa is shown in the bottom left. The inset shows emission spectra of a GeSnOI microdisk mesa with a 5 μm diameter, below and above lasing threshold, at 20°C.

We started our investigation of lasing at 273 K, i.e. the highest lasing temperature reported in the literature. Figure 3 shows the emission spectra of a GeSnOI microdisk mesa with a 5 μm diameter for different pump power densities, with a clear transition from a spontaneous emission regime to lasing, also noticeable in the Light in-Light out curve in the inset. The threshold density at 273 K was 240 kW cm^{-2} and lasing occurred at 0.355 eV, in line with the $TE_{11,1}$ whispering gallery mode resonance (at 0.358 eV from modeling). The adjacent $TE_{10,1}$ and $TE_{12,1}$ modes were indeed at 0.333 eV and 0.38 eV (free spectral range around 25 meV), without a good overlap with the maximum of optical gain.

The WGM resonances of the microdisk were calculated a two-dimensional (2D) analytical model, as described in Ref. [3]. The resonance wavelength of the cavity mode with azimuthal index m was calculated from the roots of the mth Bessel function $I_m\left(\frac{2\pi n_{eff}(\lambda)}{\lambda_{res}}a\right)$. The optical field was plotted at the resonant wavelength to obtain the corresponding radial number of nodes, n, along the disk radius (a). To account for the modal dispersion of vertically confined modes, the

Optics EXPRESS

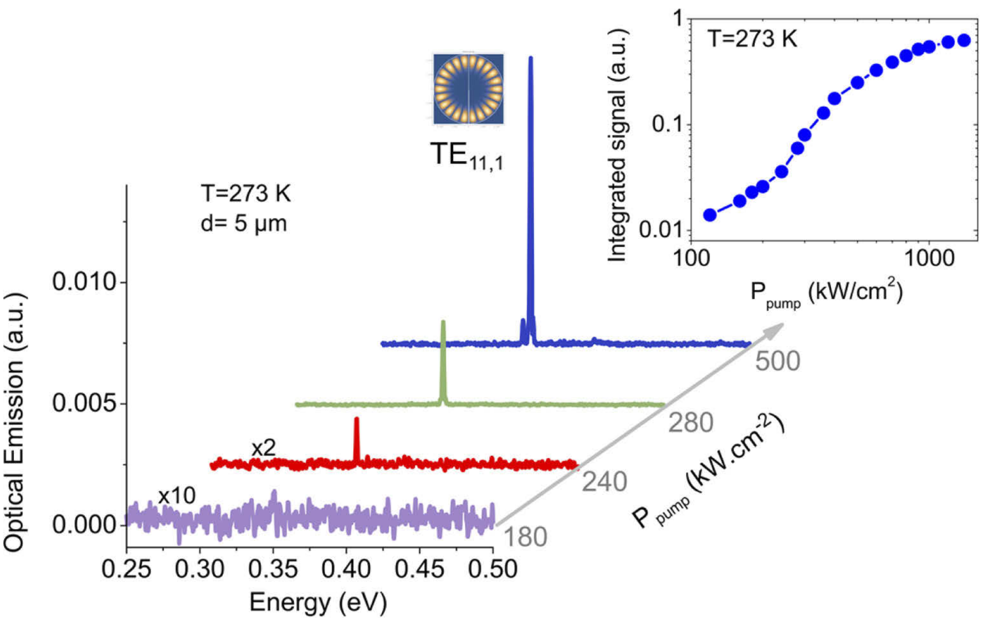

Fig. 3. Emission spectra at 273 K under different excitation densities, up to 500 kW.cm^{-2}, of a GeSnOI microdisk mesa with a 5 µm diameter. The $TE_{11,1}$ lasing whispering gallery mode profile is shown in the graph. The right inset shows the Light in-Light out curve (Log-Log scale).

effective index $n_{eff}(\lambda)$ was obtained from 1D slab modeling of TE-polarized waves propagating in the GeSn layer. This 2D analytical model perfectly reproduced the WGM resonances obtained with the aperiodic Fourier modal method, as detailed in Ref. [14].

The lasing spectra under excitation higher than 500 kW cm^{-2}, as shown later on, become multimode due to the optical gain spectral and spatial broadenings. A similar behavior was reported in Ref. [6]. While this feature is generally explained in terms of homogeneous or inhomogeneous broadenings, we emphasize that the spectral range with net positive gain is spectrally narrow at high temperature, resulting in a drastic mode selection as shown thereafter.

Figure 4(a) shows the emission spectra of the 5 µm diameter microdisk mesa when the temperature increases, starting from 273 K under a fixed pump power of 880 kW cm^{-2}. At this pump density, the lasing spectra are multimode between 273 K and 285 K. Above 290 K, lasing occurs preferentially with the $TE_{11,1}$ mode, i.e. the mode associated with the onset of lasing at 273 K. Lasing is maintained up to 300 K and quenched at 303 K. This represents a major achievement since room temperature lasing is demonstrated here. Figure 4(b) shows the emission spectra as a function of pump power density at fixed heating temperature of 298 K. The corresponding Light-in Light-out (L-L) curve of the integrated signal is shown in the inset. As already observed at 273 K, a clear laser transition is observed at a threshold density of 400 kW cm^{-2}, as also shown by the S-shape of the L-L curve plotted on a Log-Log scale. Above the lasting threshold, the peak linewidth is ~ 1 meV only. It is comparable to the lasing peak linewidth of 0.5 meV for GeSnOI microdisk mesa at much lower temperatures, i.e. 74 K under similar pumping excitations [9]. Furthermore, there is a clear linewidth narrowing of the lasing peak by a factor close to two, as shown in the inset of Fig. 4(b). According to the Schawlow-Townes theory, a linewidth reduction by a factor of 2 is a signature of the transition from spontaneous emission to coherent emission.

Optics EXPRESS

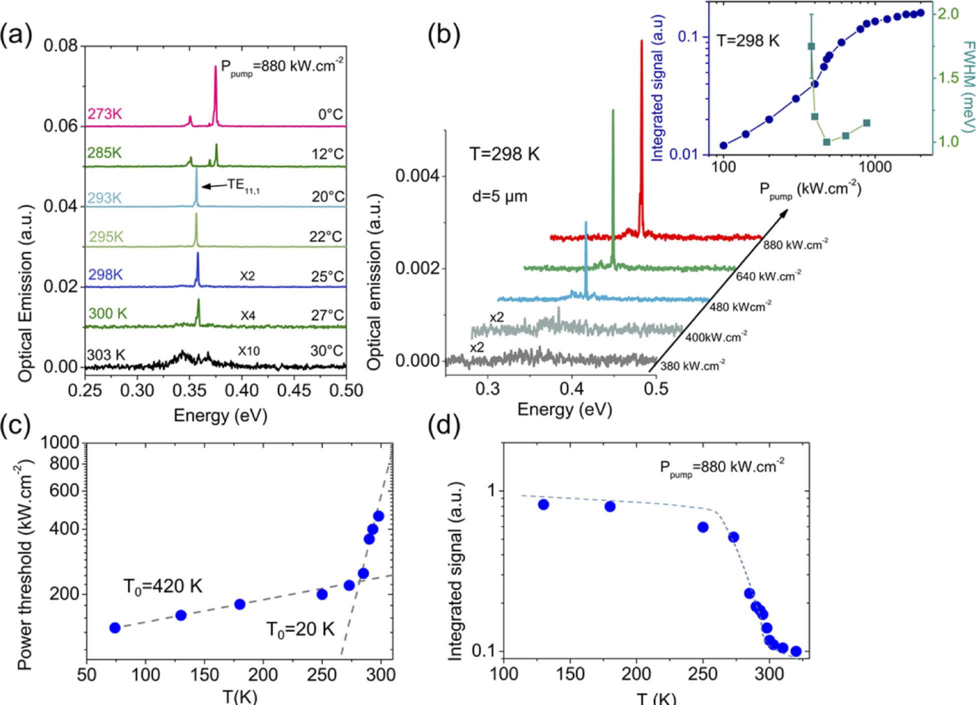

Fig. 4. (a) Temperature dependence, from 273 K up to 303 K, of the optical emission spectra under 880 kW cm^{-2} optical excitation. Lasing is maintained up to 300 K and quenched at 303 K (b) Emission spectra for different excitation densities at a fixed cooling temperature of 298 K. The right inset shows the integrated signal Light in-Light out curve (Log-Log scale) together with the lasing mode linewidths extracted from emission spectra at different pumping powers. The error bar accounts for the lower signal-to-noise ratio below threshold. (c) Lasing threshold as a function of temperature. Dashed lines are exponential fits with T_0 characteristic temperatures of 420 K and 20 K, respectively. (d) Integrated signal as a function of temperature for a fixed pump power density of 880 kW cm^{-2}.

We studied the lasing threshold as a function of temperature over a wider range of temperature as shown in Fig. 4(c). From 75 K up to 273 K, lasing characteristics are stable and the threshold increases only by a factor of two. In that temperature range, the threshold increase is well accounted by an exponential law with a characteristic T_0 temperature as high as 420 K, i.e. 1.4 times T_{room} with a room temperature of 293 K. Such a characteristic shows that the optical gain should potentially be maintained above room temperature. However, above 273 K, the slope abruptly changes and the threshold increases much more rapidly, with a T_0 of 20 K only, then. The slope change above 273 K occurs simultaneously with the onset of a laser signal decrease, as shown in Fig. 4(d). This steep decrease of the signal and the abrupt threshold increase suggest that thermal activation of extra losses occurs in the gain region of the cavity. The laser quenching may be due to carrier losses because of thermal activation of non-radiative processes, for instance on the microdisk mesa sidewalls through photo-induced desorption or adsorption of contaminants, as shown in Ref. [15]. Indeed, lasing whispering gallery modes are close to the microdisk etched sidewalls and should be sensitive to surface contamination there. It should be noted that the $TE_{11,1}$ mode has the lowest lasing threshold at 273 K and thus the best combination of Q-factor, spectral and spatial overlap with optical gain, enabling it to still lase at higher temperatures. Other studies, beyond the scope of this work, would be

helpful to better assess the role of surface contamination on lasing characteristics above 273 K. Effective surface passivation of GeSn as proposed in Ref. [16] would be helpful in the future to optimize the device performance robustness against temperature. Beyond the detrimental impact of non-radiative surface recombination, the material could also present bulk defects, like p-type vacancies as evidenced in Ref. [17], that may contribute to the fast laser quenching with temperature above 300 K. In view of multiple unknown parameters related to material growth conditions and processing, the fine modeling of optical gain in GeSn as a function of temperature will require further experimental analysis to build a robust model.

4. Discussion

Since lasing is a highly non-linear process involving optical gain and carrier recombination dynamics, a slight change of conditions can have a strong impact, explaining its abrupt quenching with temperature. Additional heating from the optical pump, that has to be increased to reach higher thresholds, contributes to this quenching. We can assume that the use of heterostructures, with for instance SiGeSn ternary alloys as barriers [18,19,20] would be helpful to reduce surface recombination and maintain lasing at higher temperatures with a reduced threshold. With the GeSnOI approach, there is indeed no need to suspend the layer as in [20] [21] under-etched microdisks, resulting in a better thermal management. The interest of the GeSnOI approach was also proven in [22] by bonding GeSn microdisks on SiO_2 layers (with Al_2O_3 intermediate layers and no residual compressive strain, afterwards). Another advantage of the GeSnOI platform that is thoroughly discussed in [22] is the removal of interfacial defects between the GeSn active layer and the Ge strain buffer layer underneath, significantly improving the laser thresholds characteristics in Refs. [9] and [6]. The low-temperature thresholds of the structures investigated here are larger than those reported in Refs. [6] and [9]. The later used lower tin content as gain media and lasing occurred at shorter wavelength, i.e. smaller than 2.4 µm against 3.54 µm here, with then lower free carrier absorption losses. However, the robustness versus temperature is much stronger here because of a significantly higher Sn content, and higher directness of the band structure, a better thermal management and the use of shorter optical pulses.

We have shown that the room temperature hurdle for lasing with GeSn alloys can be overcome. Our GeSnOI approach enabled to fabricate smaller micro-resonators than in [7] and [8], potentially enabling their dense integration on a semiconductor-on-insulator photonic platform as shown in [23]. Further optimizations of the GeSn structural quality, with for example a step graded increase of the Sn content during growth, as in [7] or [24], and the right surface passivation strategy should result in even better performances.

In the near future, one of the main challenges will be to fabricate electrically-pumped devices taking full advantage of the GeSnOI technology. Pin GeSn diodes will then have to be grown and bonded with the process flow shown here. The design of the laser cavity will have to be adapted in order to minimize losses due to the use of metallic electrodes while having the best possible carrier injection in the gain region. We have used here a cavity design, but many other designs, like conventional Fabry-Perot ridge cavities, could be thought of. Our strategy is indeed compatible with complex heterostructures and electronic band engineering, as in Ref. [2] with 100 K electrically pumped lasers.

5. Conclusion

To conclude, we have shown here that room temperature lasing can be obtained with thick GeSn alloys with a tin content of 17% thanks to the use of a GeSnOI specific technology with interfacial misfit dislocations removal, strain engineering, improved optical confinement and thermal management. In numerous previous works with the same tin content alloys and lasers fabricated from as-grown GeSn/Ge-SRB/Si, room temperature lasing was not reached despite

advanced SiGeSn/GeSn heterostructures engineering [7–8,24–26]. The current study emphasizes the potential of the GeSnOI technology.

Funding. Agence Nationale de la Recherche (ANR-17-CE24-0015).

Disclosures. The authors declare that there are no conflicts of interest related to this article.

Data availability. Data underlying the results presented in this paper are not publicly available at this time but may be obtained from the authors upon reasonable request.

References

1. S. Wirths, R. Geiger, N. von den Driesch, G. Mussler, T. Stoica, S. Mantl, Z. Ikonic, M. Luysberg, S. Chiussi, J. M. Hartmann, H. Sigg, J. Faist, D. Buca, and D. Grützmacher, "Lasing in direct-bandgap GeSn alloy grown on Si," Nat. Photonics **9**(2), 88–92 (2015).
2. Y. Zhou, Y. Miao, S. Ojo, H. Tran, G. Abernathy, J. M. Grant, S. Amoah, G. Salamo, W. Du, J. Liu, J. Margetis, J. Tolle, Y. Zhang, G. Sun, R. A. Soref, B. Li, and S.-Q. Yu, "Electrically injected GeSn lasers on Si operating up to 100 K," Optica **7**(8), 924–928 (2020).
3. A. Elbaz, D. Buca, N. von den Driesch, K. Pantzas, G. Patriarche, N. Zerounian, E. Herth, X. Checoury, S. Sauvage, I. Sagnes, A. Foti, R. Ossikovski, J.-M. Hartmann, F. Boeuf, Z. Ikonic, P. Boucaud, D. Grützmacher, and M. El Kurdi, "Ultra-low-threshold continuous-wave and pulsed lasing in tensile-strained GeSn alloys," Nat. Photonics **14**(6), 375–382 (2020).
4. D. Rainko, Z. Ikonic, A. Elbaz, N. von den Driesch, D. Stange, E. Herth, P. Boucaud, M. El Kurdi, D. Grützmacher, and D. Buca, "Impact of tensile strain on low Sn content GeSn lasing," Sci. Rep. **9**(1), 259 (2019).
5. S. Al-Kabi, S. A. Ghetmiri, J. Margetis, T. Pham, Y. Zhou, W. Dou, B. Collier, R. Quinde, W. Du, A. Mosleh, J. Liu, G. Sun, R. A. Soref, J. Tolle, B. Li, M. Mortazavi, H. A. Naseem, and S.-Q. Yu, "An optically pumped 2.5 μm GeSn laser on Si operating at 110 K," Appl. Phys. Lett. **109**(17), 171105 (2016).
6. A. Elbaz, R. Arefin, E. Sakat, B. Wang, E. Herth, G. Patriarche, A. Foti, R. Ossikovski, S. Sauvage, X. Checoury, K. Pantzas, I. Sagnes, J. Chrétien, L. Casiez, M. Bertrand, V. Calvo, N. Pauc, A. Chelnokov, P. Boucaud, F. Boeuf, V. Reboud, J.-M. Hartmann, and M. El Kurdi, "Reduced Lasing Thresholds in GeSn Microdisk Cavities with Defect Management of the Optically Active Region," ACS Photonics **7**(10), 2713–2722 (2020).
7. J. Chrétien, N. Pauc, F. Armand Pilon, M. Bertrand, Q.-M. Thai, L. Casiez, N. Bernier, H. Dansas, P. Gergaud, E. Delamadeleine, R. Khazaka, H. Sigg, J. Faist, A. Chelnokov, V. Reboud, J.-M. Hartmann, and V. Calvo, "GeSn Lasers Covering a Wide Wavelength Range Thanks to Uniaxial Tensile Strain," ACS Photonics **6**(10), 2462–2469 (2019).
8. Y. Zhou, W. Dou, W. Du, S. Ojo, H. Tran, S. A. Ghetmiri, J. Liu, G. Sun, R. Soref, J. Margetis, J. Tolle, B. Li, Z. Chen, M. Mortazavi, and S.-Q. Yu, "Optically Pumped GeSn Lasers Operating at 270 K with Broad Waveguide Structures on Si," ACS Photonics **6**(6), 1434–1441 (2019).
9. B. Wang, E. Sakat, E. Herth, M. Gromovyi, A. Bjelajac, J. Chaste, G. Patriarche, P. Boucaud, F. Boeuf, N. Pauc, V. Calvo, J. Chrétien, M. Frauenrath, A. Chelnokov, V. Reboud, J.-M. Hartmann, and M. El Kurdi, "GeSnOI mid-infrared laser technology," Light: Sci. Appl. **10**(1), 232 (2021).
10. A. Elbaz, M. El Kurdi, A. Aassime, S. Sauvage, X. Checoury, I. Sagnes, F. Boeuf, and P. Boucaud, "Solving thermal issues in tensile-strained Ge microdisks," Opt. Express **26**(22), 28376–28384 (2018).
11. J. Aubin, J. M. Hartmann, A. Gassenq, L. Milord, N. Pauc, V. Reboud, and V. Calvo, "Impact of thickness on the structural properties of high tin content GeSn layers," J. Cryst. Growth **473**, 20–27 (2017).
12. J. M. Hartmann, A. M. Papon, V. Destefanis, and T. Billon, "Reduced pressure chemical vapor deposition of Ge thick layers on Si(001), Si(011) and Si(111)," J. Cryst. Growth **310**(24), 5287–5296 (2008).
13. P. Zaumseil, Y. Hou, M. A. Schubert, N. von den Driesch, D. Stange, D. Rainko, M. Virgilio, D. Buca, and G. Capellini, "The thermal stability of epitaxial GeSn layers," APL Materials **6**, 076108 (2018).
14. F. Bigourdan, J.-P. Hugonin, and P. Lalanne, "Aperiodic-Fourier modal method for analysis of body-of-revolution photonic structures," J. Opt. Soc. Am. A **31**(6), 1303–1311 (2014).
15. I. Rousseau, G. Callsen, G. Jacopin, J.-F. Carlin, R. Butté, and N. Grandjean, "Optical absorption and oxygen passivation of surface states in III-nitride photonic devices," J. Appl. Phys. **123**(11), 113103 (2018).
16. L. Groell, A. Attiaoui, S. Assali, and O. Moutanabbir, "Combined Iodine- and Sulfur-Based Treatments for an Effective Passivation of GeSn Surface," J. Phys. Chem. C **125**(17), 9516–9525 (2021).
17. S. Assali, M. Elsayed, J. Nicolas, M. O. Liedke, A. Wagner, M. Butterling, R. Krause-Rehberg, and O. Moutanabbir, "Vacancy complexes in nonequilibrium germanium-tin semiconductors," Appl. Phys. Lett. **114**(25), 251907 (2019).
18. D. Stange, N. von den Driesch, D. Rainko, S. Roesgaard, I. Povstugar, J.-M. Hartmann, T. Stoica, Z. Ikonic, S. Mantl, D. Grützmacher, and D. Buca, "Short-wave infrared LEDs from GeSn/SiGeSn multiple quantum wells," Optica **4**(2), 185–188 (2017).
19. D. Stange, N. von den Driesch, T. Zabel, F. Armand-Pilon, D. Rainko, B. Marzban, P. Zaumseil, J.-M. Hartmann, Z. Ikonic, G. Capellini, S. Mantl, H. Sigg, J. Witzens, D. Grützmacher, and D. Buca, "GeSn/SiGeSn Heterostructure and Multi Quantum Well Lasers," ACS Photonics **5**(11), 4628–4636 (2018).
20. Q. M. Thai, N. Pauc, J. Aubin, M. Bertrand, J. Chrétien, V. Delaye, A. Chelnokov, J.-M. Hartmann, V. Reboud, and V. Calvo, "GeSn heterostructure micro-disk laser operating at 230 K," Opt. Express **26**(25), 32500–32508 (2018).

Optics EXPRESS

21. D. Stange, S. Wirths, R. Geiger, C. Schulte-Braucks, B. Marzban, N. von den Driesch, G. Mussler, T. Zabel, T. Stoica, J.-M. Hartmann, S. Mantl, Z. Ikonic, D. Grützmacher, H. Sigg, J. Witzens, and D. Buca, "Optically Pumped GeSn Microdisk Lasers on Si," ACS Photonics **3**(7), 1279–1285 (2016).
22. D. Burt, H.-J. Joo, Y. Jung, Y. Kim, M. Chen, Y.-C. Huang, and D. Nam, "Strain-relaxed GeSn-on-insulator (GeSnOI) microdisks," Opt. Express **29**(18), 28959–28967 (2021).
23. H.-J. Joo, Y. Kim, D. Burt, Y. Jung, L. Zhang, M. Chen, S. J. Parluhutan, D.-H. Kang, C. Lee, S. Assali, Z. Ikonic, O. Moutanabbir, Y.-H. Cho, C. S. Tan, and D. Nam, "1D photonic crystal direct bandgap GeSn-on-insulator laser," Appl. Phys. Lett. **119**(20), 201101 (2021).
24. J. Margetis, S. Al-Kabi, W. Du, W. Dou, Y. Zhou, T. Pham, P. Grant, S. Ghetmiri, A. Mosleh, B. Li, J. Liu, G. Sun, R. Soref, J. Tolle, M. Mortazavi, and S.-Q. Yu, "Si-Based GeSn Lasers with Wavelength Coverage of 827–833 µm and Operating Temperatures up to 180 K," ACS Photonics **5**(3), 827–833 (2018).
25. V. Reboud, A. Gassenq, N. Pauc, J. Aubin, L. Milord, Q. M. Thai, M. Bertrand, K. Guilloy, D. Rouchon, J. Rothman, T. Zabel, F. Armand Pilon, H. Sigg, A. Chelnokov, J. M. Hartmann, and V. Calvo, "Optically pumped GeSn micro-disks with 16% Sn lasing at 3.1 µm up to 180 K," Appl. Phys. Lett. **111**(9), 092101 (2017).
26. W. Du, Q. M. Thai, J. Chrétien, M. Bertrand, L. Casiez, Y. Zhou, J. Margetis, N. Pauc, A. Chelnokov, V. Reboud, V. Calvo, J. Tolle, B. Li, and S.-Q. Yu, "Study of Si-Based GeSn Optically Pumped Lasers With Micro-Disk and Ridge Waveguide Structures," Front. Phys. **7**, 147 (2019).

193.55.30.22 {ts '2022-02-01 10:36:27'}